RAA 2020 Vol. **20** No. **12**, 200(8pp) doi: 10.1088/1674-4527/20/12/200

http://www.raa-journal.org *http://iopscience.iop.org/raa*

***R**esearch in*
***A**stronomy and*
***A**strophysics*

Research and application of reanalysis data for radio astronomical site testing

Ming-Shuai Li[1,2], Rui Li[1,2], Na Wang[1,2⋆] and Xing-Wu Zheng[3]

[1] Xinjiang Astronomical Observatory, Chinese Academy of Sciences, 830011 Urumqi, China; *na.wang@xao.ac.cn*
[2] Key Laboratory of Radio Astronomy, Chinese Academy of Sciences, 210034 Nanjing, China
[3] School of Astronomy & Space Science, Nanjing University, Nanjing 210093, China

Received 2020 March 4; accepted 2020 June 15

Abstract Selecting a good site for ground-based astronomy is very important. Based on the ERA-Interim global reanalysis data, this paper studied the atmospheric conditions of the Qitai Telescope (QTT) site from the aspects of absolute humidity, mixing ratio and precipitable water vapor (PWV). Error estimations of meteorological parameters are also analyzed. These primary results show that the QTT site has obvious advantages in terms of conditions with much less atmospheric water vapor than two well-known existing sites with 100-meter-aperture radio telescopes in the world. In addition, due to the influence of atmospheric water vapor on radio observations, the atmospheric transmittance for each frequency band of the site are simulated, and the atmospheric opacity is also calculated as well as Planck radiation brightness. Based on these results, the effective observational time of different bands is further estimated.

Key words: site testing — opacity — radiative transfer

1 INTRODUCTION

Major achievements in astronomy are closely related to the improvement of observational equipments, such as the design of new technology for telescopes and application of high-sensitivity detectors. However, good equipment must be installed at a site with excellent atmospheric conditions to be fully efficient. Astronomers not only carefully design large telescopes, but also spend a lot of time choosing good sites. With the continuous improvement of observational equipment, influence of the atmosphere will be more prominent. Two testing campaigns in the astronomical world in the 1960s and 1980s helped people to have a better understanding (Fried 1966; Young 1974; Roddier 1981) of how to choose a good telescope site with parameters indicating the quality of a site.

Usually, for radio telescope site selection, several key factors should be considered as follows:

1. Accessibility to the site for construction and operations
   The site should be as flat or less undulating as possible, furthermore, good geological conditions for antenna foundation, sufficient power supply and necessary living and logistic conditions as well as convenient transportation are very important.
2. Radio Frequency Interference (RFI) shielding;
   Radio signals from the distant universe received by radio astronomy equipment are extremely weak. In the observed band of the telescope, any "slight" interference would be fatal to large radio telescopes (Wu et al. 2001; Han 1985; Liu et al. 2007). Therefore, the site should be kept as far away as possible from sources of interference (both artificial and natural) that could harm the operation of the telescope. Ideally, a natural terrain barrier around the site would shield the site from RFI at a distance. The Qitai Telescope (QTT) site, being an example, is located in the Tianshan Mountains, and is surrounded by ridges which form a natural shielding layer. With the implementation of Radio Quiet Zone (RQZ) legislation, the RFI suppression at the QTT site will be further enhanced.
3. Wind resistant design of radio telescope structure;
   The effect of wind load will cause the shape of the reflecting surface of the telescope to change, which will reduce the shape fitting accuracy of the reflecting surface. It can cause focal deviation and pointing error, reduce the sensitivity and resolution of the telescope, and ultimately affect its performance (see Ye & Li 1986). For the structure of a giant radio telescope, the role of wind load cannot be ignored due to its large area of reflection surface and various actual working

⋆ Corresponding author

conditions (pitch angle, wind direction angle change, etc.).

4. Annual precipitable water vapor (PWV) as small as possible for low opacity;
   The atmospheric water content over the site is the main index to measure the quality of a millimeter wavelength observation site. The fluctuation of atmospheric noise radiation caused by the fluctuation of atmospheric water content will limit the sensitivity of the telescope. For a single antenna observation, the small scale unevenness and variation of atmospheric water content in spatial distribution will also cause variation in the antenna pointing and decrease the antenna gain.

Dry sites are necessary for the successful operation of a radio telescope, which indicates long observable time. Generally, the water vapor density in the atmosphere decreases exponentially with the increase in the altitude up to 2000 m (Starr & White 1955). Therefore, in order to obtain low atmospheric water content, the site must be located in a local or a large area with a dry climate and a high enough altitude. In the field of astronomical site selection, many efforts have been done for measuring the moisture content of the atmosphere in various ways (Li et al. 2003; Qian 2011; Huang & Mao 1994; Wang et al. 2008; Wang & Zhang 2008), including in situ measurements and satellite remote sensing (Mockler 1995; Chaboureau et al. 1998) i.e., Global Positioning System (GPS), Moderate-Resolution Imaging Spectroradiometer (MODIS) and radiosondes. Matsushita et al. (2017) checked the satellite-based PWV data measured by MODIS on the NASA Aqua and Terra satellites for potential sites with respect to the locations of the available millimeter wave band telescopes, and several potential broad regions of interest were identified from the data: western regions of Xinjiang and Tibet in China, the highest mountains of southern Alaska, Greenland and northern Canada.

QTT will be one of the largest fully steerable radio telescope in the world, which will be located in Qitai County, Xinjiang, China. For the site with an altitude of around 1800 m, it will provide excellent observation conditions in the frequency range from 150 MHz to 115 GHz. The investigation of water vapor is very important for observations in the Q and W bands. We present an analysis of water vapor content characteristics, such as absolute humidity, mixing ratio and PWV. In addition, the transparency of the atmosphere was calculated, which provides a basis for further estimating the effective observation time of each band. For the QTT site, we compare these characteristics with those of Effelsberg-100 m and Green Bank Telescope (GBT)-100 m sites which enable us to better understand the scientific potential of QTT.

2 DATA AND CHARACTERIZATION PARAMETERS

Raw data are from the European Centre for Medium-Range Weather Forecasts (ECMWF) reanalysis datasets (Hersbach et al. 2018) which have proved to be applicable in the field of climate and weather research (Meng et al. 2018; Wei et al. 2015; Yuan et al. 2012; Rienecker et al. 2011). Here, reanalysis means to control and assimilate the observation data from various sources (ground, ship, radiosonde, anemometry balloon, aircraft, satellite, etc.) and obtain a complete set of reanalysis data. The ECMWF data are regridded with a lat/lon resolution of $0.25^\circ \times 0.25^\circ$ and a time resolution of 3 hours for 37 barometeric layers (Kobayashi et al. 2009). ECMWF data for the five-year period (2014 – 2018) were first interpolated to the observatory latitude and longitude to get the vertical profiles for our model. Quantile statistics of the temperature, pressure, H_2O mixing ratio, height, etc. were then calculated in the whole period, including all times of day, for each barometric layer.

The moisture content of the atmosphere can be described by three indicators: (1) absolute humidity, which is the mass of water vapor per unit volume of air; (2) mixing ratio, the ratio of water gas quality to dry air mass per cubic meter; (3) the content of water vapor is also measured by the PWV, which is defined as the water on the measurement path of the unit section, compressed into a layer of water with a certain thickness per unit area.

2.1 Absolute Humidity

Absolute humidity (AH) is a parameter derived from the water vapor equation of state. The derivation process is summarized as the following:

1. Saturated vapor pressure is described as
$$e_s = e_{s0}[\frac{a(T-273.5)}{T-b}] = e_{s0}[\frac{at}{273.5+t-b}], \quad (1)$$
   where t is air temperature, T is the absolute temperature and e_s is saturated water vapor pressure. a = 17.269, b = 35.86, if $t > -15^\circ$ C, otherwise a = 21.875, b = 7.66. e_{s0} is a constant value e_{s0} = 6.11 hPa ($t = 0^\circ$ C).
2. Relative humidity (RH)
$$\mathrm{RH} = \frac{e}{e_s} \times 100\%. \quad (2)$$
   According to the ideal gas law, the AH is defined by
$$\mathrm{AH} = \frac{e}{R_\omega T} = 217\frac{e}{T}(g\,m^{-3}), \quad (3)$$

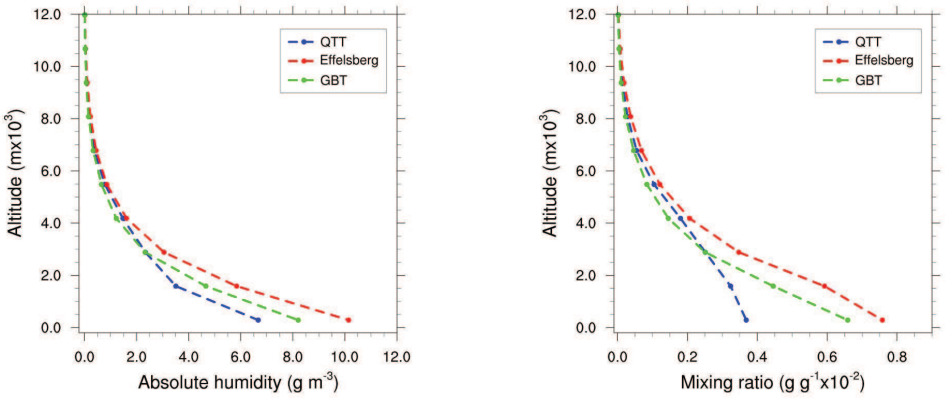

Fig. 1 Plot of AH (a) and MR (b) varying with height from the years 2014 to 2018.

where e is water vapor pressure in the air and R_ω is the ideal gas constant. It can be obtained by combining (1)∼(3).

2.2 Mixing Ratio

The mixing ratio (MR) describes the ratio of wet particles to dry particles in the air. It is derived from the specific humidity q which is obtained from global reanalysis data.

$$q = \frac{m_v}{m_v + m_d} = \frac{0.622e}{p - 0.378e}, \tag{4}$$

$$\mathrm{MR} = \frac{m_v}{m_d} = \frac{0.622e}{p - e} = \frac{q(p - 0.378e)}{p - e}. \tag{5}$$

Here m_v is the mass of wet air, m_d is the mass of dry air and p is atmospheric pressure.

Based on meteorological theory, a large portion of the lower-level water vapor (elevation below 2000 m) is affected by the topography and geomorphology (Orlanski 1975), such as the rivers and lakes or native vegetation. The QTT site is located at the northern foot of the East Tianshan Mountains of Xinjiang, an area that has a typical continental climate, and humidity is very low throughout the year. The average annual precipitation in the region is 145 mm (Cui & Hai 2005; Liu et al. 2010), which is only 23% of the national average level, while the evaporation in Xinjiang is about 2000 mm on average, which is much higher than the national average (Su et al. 2003). The surrounding mountain ridge varies in altitude from 1860 m to 2250 m and forms a 2 km×4 km basin. Figure 1(a) demonstrates that in the vicinity of an altitude of 2000 m, the AH of the QTT site is less than 3.15 g m^{-3}, while the values at Effelsberg and the GBT site are close to 4 g m^{-3} and 5 g m^{-3} respectively. Moreover, with the decrease in altitude, the trend of AH is comparatively stable and the AH value of the QTT site remains lower than that at the other two stations. It further indicates by MR in Figure 1(b) that as the altitude increases, the proportion of water vapor in the same air quality unit changes significantly, compared to the dry air quality: the MR value of the QTT site drops rapidly within the maximum range of 0.0036 g g^{-1}, and the values of the Effelsberg and GBT sites are generally higher than at the QTT site, with a larger maximum range around 0.0076 g g^{-1}. The middle-and upper-level water vapor contents (above an altitude of 2000 m) are mainly related to large-scale circulation and exhibit little difference among the global range (Orlanski 1975). Based on the results, it can be concluded that moisture content of the atmosphere as indicated by AH and MR in the QTT site is lower than at the GBT and Effelsberg sites.

2.3 PWV

PWV is an indicator of water vapor quantity in the atmosphere. The reanalysis data provide stratified atmospheric pressure and specific humidity over the selected area. The theoretical method integrates specific humidity q along atmospheric pressure p.

$$\mathrm{PWV}(\lambda, \varphi, \mathrm{t}) = \frac{1}{g} \int_{p_s}^{p} q \, dp \,. \tag{6}$$

Here λ and φ represent longitude and latitude respectively, t is the time span of data, and g is the gravitational acceleration of the Earth. For the QTT site, $\lambda = 89.6824°$ E, $\varphi = 43.6011°$ N and t is from years 2014 to 2018. The integration is from the ground to the upper troposphere.

Figure 2 displays the distribution of the monthly mean PWV value averaged from the years 2014 to 2018 at the QTT site. It is clear that there is a seasonal variation, in which winter is lower than summer, and January seems to have the best water vapor condition around 1.95 mm, while July remains the worst, with a value of 14.44 mm.

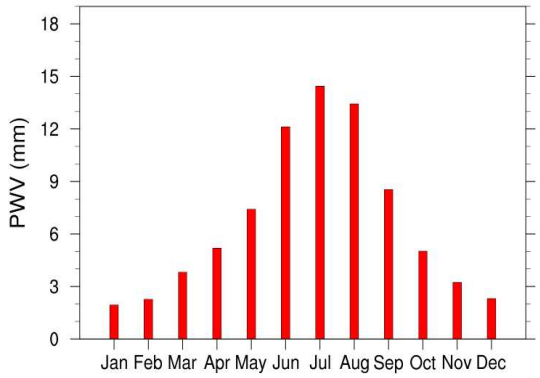

Fig. 2 Monthly average distribution of PWV for the QTT site.

The distributional characteristics of PWV are very close in spring and autumn, but spring is slightly higher than that in autumn, which is influenced by the atmospheric circulation (Gao et al. 2003). Some studies (Nan et al. 2003) revealed that spring precipitation in northwest China has more disturbance factors and strong updraft, which provides advantages for precipitation. In autumn, the Xinjiang ridge and the middle Siberian ridge are relatively stable, which is not suitable for precipitation.

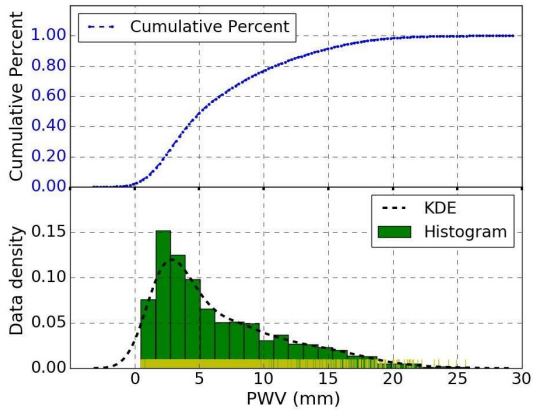

Fig. 3 Historical distribution of PWV at the QTT site.

Figure 3 presents the cumulative distribution and histograms of the PWV. It affirms that the PWV of the QTT site is mostly less than 20 mm, and more than half of the PWV records are less than 5 mm, and 80% of the water vapor is concentrated below 10 mm. Combined with Figure 2, the histograms suggest that the PWV conditions below 4 mm mostly occurred in winter, accounting for more than 40% throughout the year. We then compared the distribution of PWV using our 5 year period statistics with those at the GBT in the United States and the Effelsberg telescope in Germany, which are well-established sites for astronomical observations. The results from Figure 4 demonstrate that the water vapor distribution curves of the Effelsberg and GBT sites are very similar, and tend to be

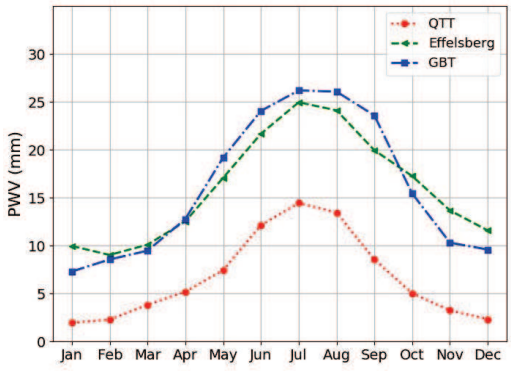

Fig. 4 The statistical distribution of PWV from the QTT, GBT and Effelsberg sites.

consistent from February to April. In general, the PWV of GBT is slightly higher than that at Effelsberg in summer and opposite in winter. The annual averages are 15.98 mm and 16.04 mm respectively, which are significantly higher than the average value of 6.64 mm for the QTT site. This further shows that the PWV of the QTT site is far lower than the previous two records according to the monthly average; especially in January, PWV values of the Effelsberg and GBT sites are 9.95 mm and 7.29 mm respectively, which are 4–5 times that at the QTT site. In July, the PWV values of the Effelsberg and GBT sites are 24.95 mm and 26.19 mm respectively, which are also higher than QTT's value of 14.44 mm. Therefore, the water vapor conditions of the QTT site are systematically lower than the corresponding values at the Effelsberg and GBT sites in the whole year.

2.4 Error Estimates of Reanalysis Datasets

Earlier studies have tested the quality and reliability of reanalysis data from different perspectives and derived a large number of comparative analysis data (Jia et al. 2014; Hu et al. 2013; Chen et al. 2015). The PWV retrieved by the CE-318 sun photometer is correlated with the radiosonde data (Zhang et al. 2006; Hu et al. 2014), hence it is also sensible to obtain the PWV by the CE-318 sun photometer. We first compared PWV data obtained from ECMWF with the CE-318 sun photometer located at the QTT site, and found that the minimum absolute deviance is 0.07 mm, which occurred in winter, and the maximum absolute deviance is 4.03 mm, which occurred in summer. The relative deviation range is 0.2% – 22%, which is partially due to the duration of operation of the CE-318 sun photometer, because data monitoring is only available in the daytime and on clear days. Additionally, insufficient calibration of the equipment will introduce extra measurement error.

We compared the RH and MR values derived from the reanalysis data with the radiosonde data in China (Yu et al. 2016; Zhang et al. 2018). The ranges of the relative deviance are 4% – 8.62% and 4% – 13%, respectively. The differences in the upper troposphere are larger than those in the lower troposphere. Meanwhile, the differences in spring and autumn are more significant than those in summer.

3 ESTIMATION OF OPACITIES AND PLANCK BRIGHTNESS TEMPERATURE AT DIFFERENT FREQUENCIES

Atmospheric water vapor is the main limiting factor of atmospheric transparency in the millimeter and sub-millimeter wavelength spectral windows, and atmospheric transparency is fundamental to the site characterization (Radford 2011). If cosmic radiation does not penetrate the atmosphere effectively, the astronomical observation will be in vain. Up to now, there is no good strategy to improve the inherent transparency of the atmosphere over the site. At the same time, atmospheric absorption leads to two negative effects: The reduction of the signal intensity by simple atmospheric absorption and introduction of noise by re-radiation at the operating temperature of the absorber (Penzias & Burrus 1973) will cause deterioration in receiver noise temperature owing to the absorptive elements. Therefore, any small improvement in transparency can greatly improve the observation efficiency. This is because the integration time is proportional to the square of the system noise. In order to further explore the impact of QTT atmospheric water vapor content on future radio astronomical observations as well as water vapor absorption in the millimeter wave bands, atmospheric models (AMs) were investigated in our work, and atmospheric opacity, transmittance and radiant brightness temperature were analyzed.

Previously, several AMs were used for radio- and far-infrared astronomy, including not only air-borne applications but also ground based observatories. The models of MOLIERE (Urban 2004), ATRAN (Lord 1992) and AM (Paine 2019) have been investigated by Guan et al. (2012) on the GREAT/SOFIA (Becklin & Gehrz 2009; Heyminck et al. 2012) calibration. By comparing the three models, the result indicates that the atmospheric opacity is higher for MOLIERE and ATRAN due to these collision-induced absorption (CIA) processes that differ by a factor of $\simeq 2$ between MOLIERE and AM, and ATRAN does not include the CIA from N_2 and O_2, which is responsible for the quasi-continuum opacity present in the other two models. Although ATRAN has some tiny deviations in the frequencies of a few higher excitation waterlines, the three models are consistent in the opacity of a wet-atmosphere. This is because the opacity of the dry-atmospheric continuum is not included in ATRAN, and even for the AM model, the distribution of the dry-atmospheric opacity caused by the CIA-process is too high compared with the observed sky radiation. Therefore, we applied the AM for QTT site analysis.

3.1 Model Introduction

The AM (Paine 2011b, 2019) is compiled by the Smithsonian Astrophysical Observatory (SAO), a special tool for calculating atmospheric radiation, suitable for spectral analysis from microwave to submillimeter, and parameter calculation including path radiation, absorption, saturation depth, etc. AM was first utilized as a space astronomical observation application to calculate the effects of the Earth's atmosphere, and was applied well in many assessments such as Mauna Kea in Hawaii. It is based on the static atmospheric layering theory, and combined with HITRAN (Lu et al. 2013; Rothman et al. 2009) database spectral parameters for line-by-line, layer-by-layer simulation, with high resolution and accuracy.

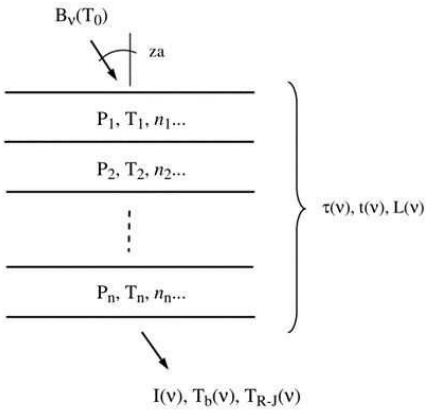

Fig. 5 The AM layer model.

The propagation diagram of AM is illustrated in Figure 5. At the beginning, the radiation has a Planck spectrum with a background temperature of T_0, which propagates through a series of layers. The parametrizations of the pressures P and temperatures T in different layers applied in AM are defined at the layer midpoints, and are presumed constant at each layer. Each layer contains various species, the type and column density of which are defined respectively. The basic spectral quantities calculated by AM are also expressed in Figure 5, which not only include properties of the layer stack, such as the propagation delay, opacity (optical depth) and transmittance, but also spectral properties of the radiation in any layer that includes Rayleigh-Jeans brightness temperature and Planck brightness temperature.

Table 1 Candidate Bands

Band	Frequency (GHz)	Scale factor	PWV (mm)
		winter (summer)	
13 mm	18 - 26.5	6.4 (1.2)	12.1 (14.5)
7 mm	30 - 50	2.7 (1.0)	6.1 (10.1)
3 mm	80 - 115	2.1 (0.6)	5.0 (7.2)

3.2 Model Application for QTT Data

Using our reanalysis data and radiative transfer program AM, we estimated the atmospheric transmission spectra from 0 GHz to 115 GHz in both winter and summer for the QTT site. Here we define winter as between the beginning of October and the end of March, and summer as April through November. First, from the ECMWF reanalysis data interpolated to the location of the QTT site, we extract profiles of the temperature, dry air quality, H_2O mixing ratio and O_3 mixing ratio at each pressure level.

Two AM configuration files were then suitably constructed for winter and summer, respectively. Here, several command-line parameters of the configuration files need to be set for our model, including the frequency grid range and resolution, ground temperature, zenith angle of observation and the scale factor which was applied to the tropospheric water vapor profile. This scale factor was used to simulate the change of PWV over the astronomical site in a way which is similar to natural change of the H_2O mixing ratio profile, and different scale factors will automatically generate corresponding PWV values through AM simulation calculation. Three reference bands of the QTT were selected for analyzing the frequency range, and they are given in the second column of Table 1.

We intend to set the transmittance T_x as a criterion: if the transmittance is greater than 90%, the corresponding spectrum accounts for more than 75% of the reference spectral range (see Fig. 6, top panels). To meet the above criterion, the required scale factors in the tropospheric water vapor profile are 6.4, 2.7 and 2.1 in winter and 1.2, 1.0 and 0.6 in summer for 13 mm, 7 mm and 3 mm bands respectively. At the 13 mm band, the changes in both sides of T_x exhibit a symmetrically increasing distribution; and at 7 mm and 3 mm bands, T_x gradually decreases with increasing frequency. It is noteworthy that the T_x curve of the 7 mm band decreases smoothly with increasing frequency, while at the 3 mm band, T_x occasionally fluctuates with the frequency, which also reveals the complexity of water vapor at the high frequency band.

Furthermore, the atmospheric opacity tau and radiant brightness temperature T_b (see Fig. 6, bottom panels) are calculated by means of the AM at the same time. These spectra suggest that tau<0.14, T_b<36 K in the range 18–26.5 GHz, tau<0.28, T_b<60 K in the range 30–50 GHz, and tau<0.45 and T_b<85 K in the range 80–115 GHz. The waveforms have characteristics of longitudinal symmetry, compared with T_x spectra.

According to the correlation between scale factor and PWV, the PWV values were estimated for 13 mm, 7 mm and 3 mm bands. The corresponding values of PWV are 12.1 mm, 6.1 mm and 5.0 mm for winter, and 14.5 mm, 10.1 mm and 7.2 mm for summer for the three bands of 13 mm, 7 mm and 3 mm, respectively, which are expressed in the third and fourth columns of Table 1.

Combined with the QTT water vapor distribution at the QTT site, we further calculated the effective observation time of different bands each year. The effective observation days per year for the QTT project receivers in the past five years (2014–2018) are presented in Table 2. These values affirm that the effective observation days in the 13 mm band are about 180 days, the effective observation time in the 7 mm band and 3 mm band are about 157 days and 151 days in winter respectively. There seem to be two important messages here. First of all, the PWV in winter is low enough and has little affect on astronomical observations at the 13 mm band. Secondly, it indicates that the values of PWV in winter are very stable except for the relatively large fluctuations in March and October which can be verified in the 7 mm and 3 mm bands. Moveover in summer, the effective observation time is decreased due to the increase of water vapor, which are about 150 days, 119 days, 58 days respectively. The results reveal that there is considerable observation time in the 13 mm band, and combined with Figure 2, some observing opportunities still exist for 7 mm and 3 mm bands in April, May and September.

In addition to the influence of atmospheric water vapor, the influence from wind is another major limitation for high-frequency observational time because of the antenna pointing accuracy. In order to achieve the maximum observational time at 13 mm, 7 mm and 3 mm bands, the wind resistance performance indexes of QTT are set to below 6 m s^{-1}, 4 m s^{-1} and 2 m s^{-1}, respectively. According to data from the wind tower at the QTT site, the cumulative percentages of observational dates for 13 mm, 7 mm and 3 mm bands are $\leq$ 96.5%, $\leq$ 90% and $\leq$ 70%, respectively. The data statistics on wind also reveal that the gale weather is mainly concentrated in summer (87.63%) and less in winter (12.37%). Therefore, the observational time at the millimeter band will be reduced slightly, due to the influence of a small proportion of strong wind.

4 CONCLUSIONS

The distribution of water vapor is obtained in the area of the radio astronomy sites by utilizing the ECMWF (2014-2018) global reanalysis data; the moisture content

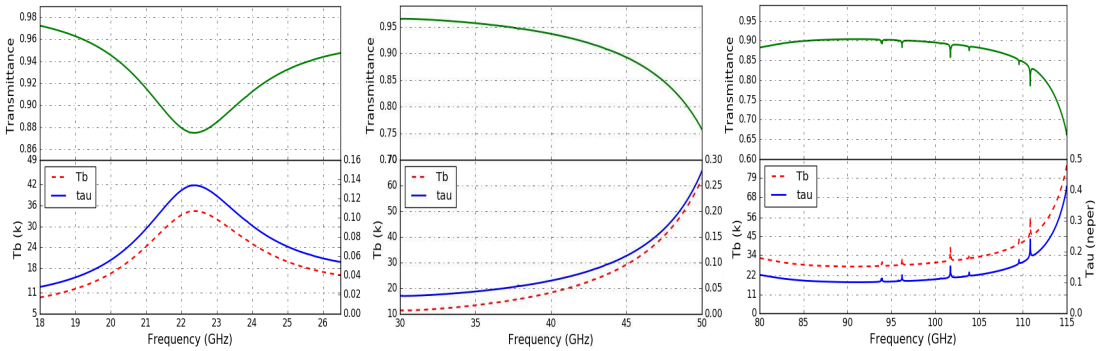

Fig. 6 Estimated atmospheric transmission spectra T_x (*top panels*), and the atmospheric opacity tau and radiant brightness temperature T_b (*bottom panels*) for the QTT site at 13 mm, 7 mm and 3 mm bands.

Table 2 Estimation of Effective Observational Days for 13 mm, 7 mm and 3 mm Bands

Band	2014		2015		2016		2017		2018	
	Winter	Summer	Winter	Summer	Winter	Summer	Winter	Summer	Winter	Summer
13 mm	179	157	182	147	181	135	182	144	181	133
7 mm	158	104	155	101	157	83	164	93	152	93
3 mm	154	55	149	50	150	38	159	40	147	49

of the atmosphere at the QTT site is relatively low by comparison, based on the AH or MR distribution, especially at altitudes below 2000 m, which has a more prominent performance. The PWV is also a few times better than other radio astronomy sites. To a great extent, this benefits from the arid-rainless climate and special terrain environment of the QTT site. The evaluation of the global reanalysis data confirmed the validity of the method. The estimated atmospheric transmission spectra suggest that most of the winter time is useable for astronomical observations at 13 mm band, and mostly effective at 7 mm band and 3 mm band. Most of summertime is useable at 13 mm band, half of the summertime is useable at 7 mm band and one third of the summertime is useable at 3 mm band. The opacity tau of the atmosphere is less than 0.14, 0.28 and 0.45 at 13 mm, 7 mm and 3 mm bands, respectively, and the radiant brightness temperature T_b is less than 36 K, 60 K and 85 K, respectively. Our results indicate that the water vapor conditions at the QTT site are low, which are ideal for astronomical observations at short centimeter and even millimeter bands.

In this work, we setup a quantitative assessment method based on the AM. With the variation of transmittance, the effect of corresponding atmospheric water vapor on astronomical observations in each band will be significantly different. This method could be applied for future telescope operation, guiding the strategy of a dynamic schedule based on the actual weather conditions and antenna performance.

Acknowledgements We would like to thank professor Jianping Tang for providing assistance and cooperation in the acquisition of global reanalysis data. The reanalysis datasets used in this paper are provided by the ECMWF. We also would like to thank professor Scott Paine for providing us the AM, which assisted us in building models suitable for the QTT site. We are also grateful to the enthusiastic colleagues for helpful comments.

References

Becklin, E. E., & Gehrz, R. D. 2009, in Astronomical Society of the Pacific Conference Series, 417, Submillimeter Astrophysics and Technology: a Symposium Honoring Thomas G. Phillips, eds. D. C. Lis, J. E. Vaillancourt, P. F. Goldsmith, T. A. Bell, N. Z. Scoville, & J. Zmuidzinas, 101

Chaboureau, J.-P., ChéDin, A., & Scott, N. A. 1998, J. Geophys. Res., 103, 8743

Chen, Z., Yang, S., & Liu, L. K. 2015, Meteorological Monthly, 41, 72, (in Chinese)

Cui, X.-Y., & Hai, Y. 2005, Journal of Xinjiang Normal University (Social Sciences), 26, 57 (in Chinese)

Fried, D. L. 1966, Journal of the Optical Society of America (1917-1983), 56, 1372

Gao, Z. Y., Zhang, J. X., Liao, F. J., & Lin, K. 2003, Journal of desert research, 23, 581, (in Chinese)

Guan, X., Stutzki, J., Graf, U. U., et al. 2012, A&A, 542, L4

Han, P. 1985, Acta Astrophysica Sinica, 26, 89, (in Chinese)

Hersbach, H., de Rosnay, P., Bell, B., et al. 2018, ERA Report Series, doi: 10.21957/tkic6g3wm, 1

Heyminck, S., Graf, U. U., Güsten, R., et al. 2012, A&A, 542, L1

Hu, Z. Y., Ni, Y. Y., Shao, H., et al. 2013, Arid Land Geography, 36, 700, (in Chinese)

Hu, Z. Y., Bi, J. R., Huang, J. P., Shi, P. S., & Liu, Y. Z. 2014, Plateau Meteorology, 33, 232, (in Chinese)
Huang, Y. L., & Mao, J. T. 1994, Acta Astrophysica Sinica, 14, 379, (in Chinese)
Jia, B. X., Xu, H. M., & An, Y. G. 2014, Meteorological Monthly, 40, 1123, (in Chinese)
Kobayashi, S., Matricardi, M., Dee, D., & Uppala, S. 2009, Quarterly Journal of the Royal Meteorological Society, 135, 2086
Li, Z., Muller, J.-P., & Cross, P. 2003, Journal of Geophysical Research (Atmospheres), 108, 4651
Liu, H., Song, J. B., Zuo, S. Y., Peng, B., & Nan, R. D. 2007, Journal of Geological Hazards and Environment Preservation, 018, 88, (in Chinese)
Liu, R., Yang, Q., & Wang, M. Z. 2010, Journal of Arid Land Resources and Environment, 24, 77, (in Chinese)
Lord, S. D. 1992, NASA Technical Memor. 103957
Lu, C. S., Wu, Z. S., Li, H. Y., et al. 2013, Journal of Terahertz Science and Electronic Information Technology, 11, 346 (in Chinese)
Matsushita, S., Asada, K., Martin-Cocher, P. L., et al. 2017, PASP, 129, 025001
Meng, X. G., Guo, J. J., & Han, Y. Q. 2018, Journal of Marine Meteorology, 38, 91, (in Chinese)
Mockler, S. B., 1995, WATER VAPOR in the CLIMATE SYSTEM Special Report, in AGU Special Report, ISBN: 0-87590-865-9
Nan, Q. H., Yang, D., & Yang, Q. 2003, Journal of desert research, 23, 554, (in Chinese)
Orlanski, I. 1975, Bulletin American Meteorological Society, 56, 527
Paine, S. 2019, Smithsonian Astrophysical Observatory, Tech. Rep, 152, doi: 10.5281/zenodo.3406496
Paine, S. 2011, Smithsonian Climate Change Research Symposium
Penzias, A. A., & Burrus, C. A. 1973, ARA&A, 11, 51
Qian, X. 2011, Scientia Sinica Physica, Mechanica & Astronomica, 41, 896
Radford, S. J. E. 2011, in Revista Mexicana de Astronomia y Astrofisica Conference Series, 41, 87
Rienecker, M. M., Suarez, M. J., Gelaro, R., et al. 2011, Journal of Climate, 24, 3624
Roddier, F. 1981, Progess in Optics, 19, 281
Rothman, L. S., Gordon, I. E., Barbe, A., et al. 2009, J. Quant. Spec. Radiat. Transf., 110, 533
Starr, V. P., & White, R. M. 1955, J. Mar. Res, 14, 217
Su, H. C., Wei, W. S., & Han, P. 2003, Journal of Glaciolagy and Geocryolgy, 25, 174, (in Chinese)
Urban, J. 2004, J. Quant. Spec. Radiat. Transf., 83, 529
Wang, J. C., Yao, Y. Q., & Yang, G. A. 2008, Astronomical Research & Technology, 5, 404
Wang, J., & Zhang, L. 2008, Journal of Climate, 21, 2218
Wei, F. F., Tang, J. P., & Wang, S. Y. 2015, Chinese Journal Of Geophysics, 58, 383, (in Chinese)
Wu, S. Y., Qian, S. J., & Tian, W. W. 2001, Progress in Astronomy, 19, 17, (in Chinese)
Ye, S. H., & Li, Z. G. 1986, Design of Antennae' Structure, 1st ed. (Xi'an, China: Northwest Communication Engineering Institute Press)
Young, A. T. 1974, ApJ, 189, 587
Yu, J., Li, Q. X., Liao, J., Mou, R., & Li, Q. L. 2016, Meteorological Monthly, 42, 743, (in Chinese)
Yuan, S., Cheng, H., Wang, D. Y., Wu, D. C., & Zhou, J. 2012, Journal of the Meteorological Sciences, 32, 62, (in Chinese)
Zhang, S. Q., Guo, Y. J., & Wang, G. F. 2018, Acta Meteorological Sinica, 76, 289, (in Chinese)
Zhang, Y. X., Li, X. J., & Gu, X. F. 2006, Journal of Remote Sensing, 10, 749, (in Chinese)